Open access • Proceedings Article • DOI:10.1117/12.240009

Polarized light transmission through skin using video reflectometry: toward optical tomography of superficial tissue layers — Source link

Steven L. Jacques, Martin R. Ostermeyer, Lihong V. Wang, Dawn V. Stephens

Institutions: University of Texas at Austin, Rice University

Published on: 17 May 1996

Topics: Polarizing filter, Collimated light, Optical fiber, Polarization (waves) and Reflectometry

Polarized light transmission through skin using video reflectometry: toward optical tomography of superficial tissue layers

Steven L. Jacques, Martin R. Ostermeyer, Lihong V. Wang, Dawn V. Stephens

Steven L. Jacques, Martin R. Ostermeyer, Lihong V. Wang, Dawn V. Stephens, "Polarized light transmission through skin using video reflectometry: toward optical tomography of superficial tissue layers," Proc. SPIE 2671, Lasers in Surgery: Advanced Characterization, Therapeutics, and Systems VI, (17 May 1996); doi: 10.1117/12.240009

SPIE.

Event: Photonics West '96, 1996, San Jose, CA, United States

Polarized light transmission through skin using video reflectometry: toward optical tomography of superficial tissue layers.

Steven L. Jacques[1,2], Martin Ostermeyer[1], Lihong Wang[1], Dawn Stephens[2]

[1]Laser Biology Research Lab., Univ. of Texas M. D. Anderson Cancer Center, Houston, TX 77030
[2]Rice University, Houston, TX 77030

ABSTRACT

The movement of polarized light through the superficial layers of the skin was visualized using a video camera with a polarizing filter. This study constitutes a description of the impulse response to a point source of incident collimated linearly polarized light. Polarization images reject unwanted diffusely backscattered light from deeper in the tissue and the specular reflectance from the air/tissue interface.

Two experiments were conducted:

(1) Video polarization reflectometry used a polarized HeNe laser (633 nm) pointing perpedicularly down onto a phantom medium (0.900-μm dia. polystyrene spheres in water). The video camera was oriented 10° off the vertical axis and viewed the irradiation site where the laser beam met the phantom. Video images were acquired through a polarizing filter that was either parallel or perpendicular with the reference plane defined by the source, camera, and irradiation site on the phantom medium's surface. The source polarization was parallel to the reference plane. The two images (parallel and perpendicular) were used to calculate a polarization image which indicated the attenuation of polarization as a function of distance between the source and point of photon escape from the phantom. Results indicated a strong polarization pattern within ~0.35 cm (~2.2 mfp') from source. ($mfp' = 1/(\mu_a + \mu_s')$.)

(2) Optical fiber reflectometry using a polarized diode laser (792 nm) coupled to a polarization-maintaining single-mode fiber, and a multi-mode fiber collector to collect regardless of polarization. Reflectance as a function of fiber separation was measured for the source fiber oriented parallel and perpendicular with the reference plane. Results indicated that the strongest polarization propagated within ~0.43 cm (2.2 mfp') from source.

The polarization survived ~2.2 mfp', which for skin at 630-800 nm ($mfp' \approx 0.066$ cm) corresponds to 1.5 mm (or 6.4 ps of travel at the speed of light). Using 6.4 ps as a maximum time of survival, classical paths of photon transport (Feynman paths) were calculated to illustrate the expected depth of interrogation by polarized imaging. The expected mean depth of photons is about 0.36 mm at these longer wavelengths. Shorter wavelengths would result in a shorter mfp' and therefore more superficial imaging of the skin.

Polarization images offer an inexpensive approach toward 2-D acquisition of time-gated images based on the early light escaping the tissue. Polarization imaging is an opportunity for a new form of optical image especially useful for dermatology.

0-8194-2045-X/96/$6.00

1. INTRODUCTION

Video images of the skin or other tissues are usually dominated by diffusely scattered light and by specular light from the air/tissue surface. This paper considers an approach toward rejecting both these components and acquiring images based on those few photons which only interrogate the superficial layer of the tissue. The technique involves the use of polarized light delivered as a point source on the tissue. The photons spread within the tissue and escape at the tissue surface for observation by a video camera. However, the incident photons are polarized and the video camera observes through a polarizing filter. Hence, the video images are sensitive to the polarized component of the total escaping light.

This paper presents some preliminary work on the concept of video imaging using polarized light. The feasibility of such imaging is demonstrated in liquid phantoms.

Aim of this study:

To establish the behavior of polarized light transport in the reflectance mode

in order to

specify the opportunity for video polarization images

for imaging the superficial epidermis and papillary dermis.

2. BACKGROUND

The total light, I_{total}, observed escaping the tissue may be divided into two components, a diffuse component and a polarized component:

$$I_{total} = I_D + |I_P|$$

where $|I_P|$ indicates the absolute value of the polarized component, I_P, and I_D is the diffuse light component. The polarized component is defined:

$$I_P = \frac{I_{=} - I_{\perp}}{I_{=} + I_{\perp}} = \begin{cases} 1 & \text{if } I_{\perp} = 0 \\ 0 & \text{if } I_{\perp} = I_{=} \\ -1 & \text{if } I_{=} = 0 \end{cases}$$

and the diffuse component is defined:

$$I_D = I_{total} - |I_P| = \begin{cases} 1 & \text{if } |I_P| = 0 \\ 0 & \text{if } |I_P| = 1 \end{cases}$$

3. METHODS

Phantom

A phantom was prepared using water, polystyrene spheres as scatterers, and trypan blue as absorber. The optical properties were measured by video reflectometry and utilizing diffusion theory for analysis. The optical properties at the 633 nm and 792 nm were determined which corresponded to the He Ne and diode lasers used in the study.

Table 1: Optical properties of phantom
(0.900-μm-diameter polystyrene spheres in water as scatterer with Trypan blue as absorber)

wavelength	n_{water}	$n_{spheres}$	Q_{sca}	ρ [cm^{-3}]	μ_s [cm^{-1}]	g [-]	μ_s' [cm^{-1}]	μ_a [cm^{-1}]
experimental								
633 nm							6.07	0.20
792 nm					46.8			
calculated (mie theory)								
633 nm	1.3316	1.5721	1.9763	$5.6x10^9$	70.3	0.9136	6.07	0.20
792 nm	1.3290	1.5645	1.2999	$5.6x10^9$	46.3	0.8891	5.13	0.02

transport mean free path (mfp' $= 1/(\mu_a + \mu_s')$)

633 nm	0.159 cm
792 nm	0.194 cm

$\mu_s = \mu_s'/(1-g)$; density of spheres, $\rho = \mu_s/Q_{sca}/A$
geometrical cross-sectional area of spheres, $A = \pi r^2 = \pi(0.45x10^{-4}\ cm)^2 = 0.636x10^{-8}\ cm^2$

For comparison, the optical properties of bloodless dermis in the range of 630-800 nm are approximately $\mu_s \approx 15\ cm^{-1}$, $\mu_a \approx 0.25\ cm^{-1}$, which yields a mfp' of 0.066 cm. This mfp' is 2.4-fold and 3.0-fold shorter than the phantom at 633 and 792 nm, respectively.

Optical Properties of phantom:

(polystyrene spheres + trypan blue + water)

		633 nm	792 nm
absorption	μ_a	**0.20**	**0.02 cm^{-1}**
scattering	μ_s	**70.3**	**46.3 cm^{-1}**
anisotropy	g	**0.914**	**0.889**
red. scattering	μ_s'	**6.073**	**5.14 cm^{-1}**

equivalent to

skin scaled larger by 2.4-fold to 3-fold

(2.4 to 3 mm of phantom ≈ 1 mm of skin)

Experimental setup for polarized video imaging

The experimental setup is shown below. A polarized He-Ne laser beam was directed perpendicularly down onto the liquid phantom. The camera acquired light which had entered the medium then backscattered, passing through a polarizing filter in front of the camera. The images were acquired by a frame grabber using a *Macintosh* computer and the *IP Lab* software.

Two images were acquired. First, the polarizing filter was aligned with the reference plane to achieve a *parallel* image called $I_{=}$. Second, the polarizer was set at 90° with respect to the reference plane to achieve a *perpendicular* image called $I_{\perp}$. The reference plane was specified by the camera, laser, and irradiation site on the phantom's surface.

A combined image called the *polarization image*, Ip, was prepared by calculating pixel by pixel using the definition of Ip defined in section 2.

Experimental setup: video camera

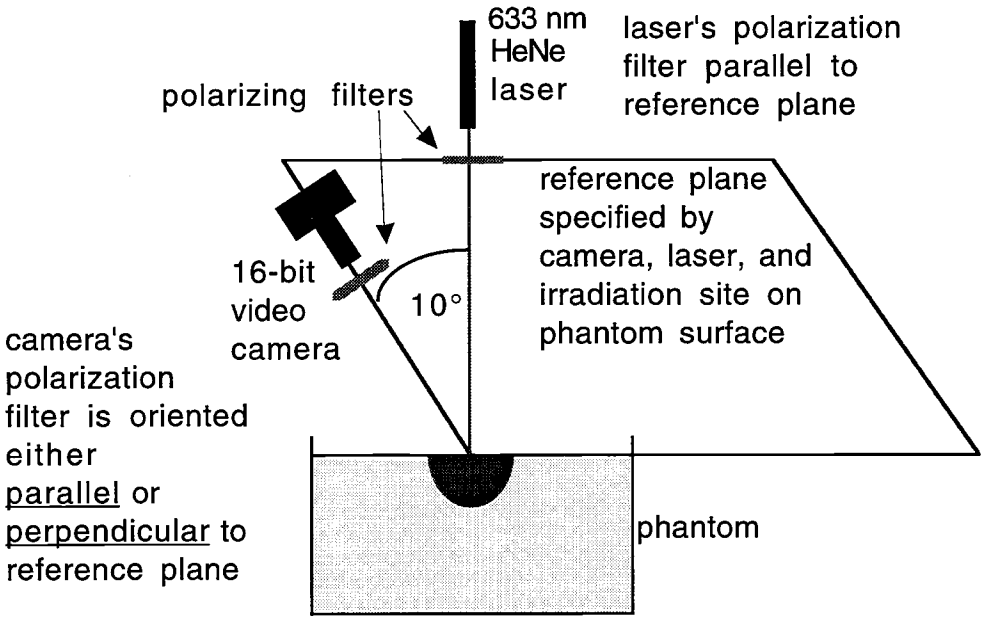

Optical fiber measurements

To provide an alternative test of the movement of polarized light in a scattering medium, a linearly polarized diode laser (792 nm) delivered via a polarization-maintaining single-mode fiber was used as a source and a second multi-mode fiber was used to collect light. The setup is shown in the figure below. The single-mode fiber preserved the polarization of the diode laser source as light was transported to the phantom. The collecting fiber collected light with equal efficiency regardless of its polarization and routed the light to an avalanche photodiode. The diode laser source was modulated at 1 MHz by a network analyzer and the diode detector output was returned to the analyzer. The modulation of the 1 MHz signal constituted the recorded data. Hence the influence of background lighting was eliminated.

Measurements were taken as a function of radial distance from the source along the medium surface. Measurements were conducted with the source fiber oriented both parallel and perpendicular to the reference plane. By comparison of the two sets of measurements, the influence of the source polarization was assessed.

Experimental setup: optical fibers

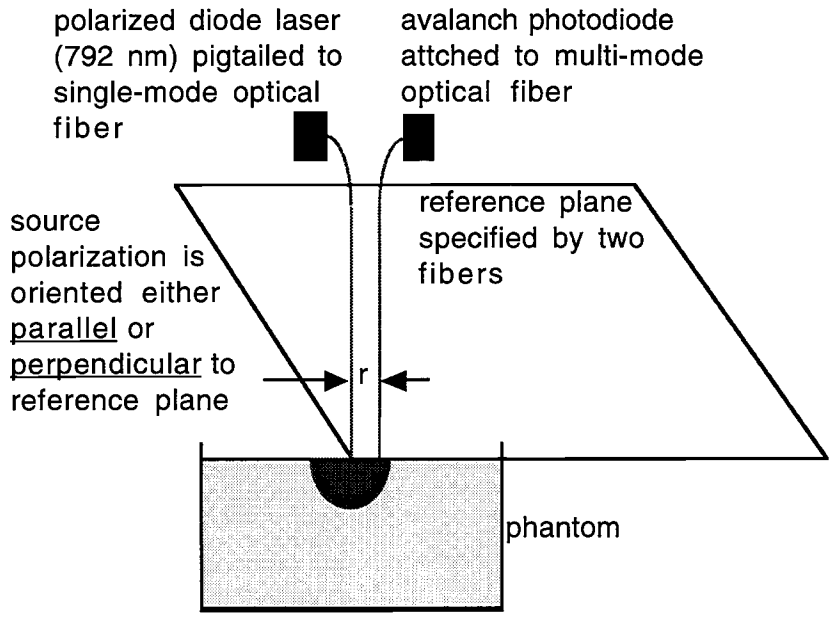

4. RESULTS

Raw images with polarized light

The raw images are shown in Figures 1, 2, and 3 for the perpendicular, parallel, and polarization images, respectively. The region of significant polarized light escape is seen as the central region of strongly anisotropic light patterns in the shape of a cross. Distant from the source, the patterns become progressively circular as the light becomes diffuse. The polarization figure based on the difference of the parallel and perpendicular images enhances this cross pattern and rejects the background diffuse light.

The parallel image shows the *cross shape* to be aligned such that one of the arms of the cross was pointed toward the camera (which is viewing from the left in the figure). The perpendicular image showed the cross shape to be aligned at 45° out of the reference plane. The polarization image enhances the cross shape.

As shown in Fig. 4, when the polarizing filter at the camera is rotated, the cross-shaped image characterizing the polarized component of the images also rotated in the same direction. The rotation of the cross shape was only half as fast as the rotation of the filter. In other words, rotating the polarizing filter 90° caused the cross shape to rotate only 45° in the same direction. Rotating the polarizing filter 180° causes the cross shape to rotate 90°, but this shape is identical to the original cross shape.

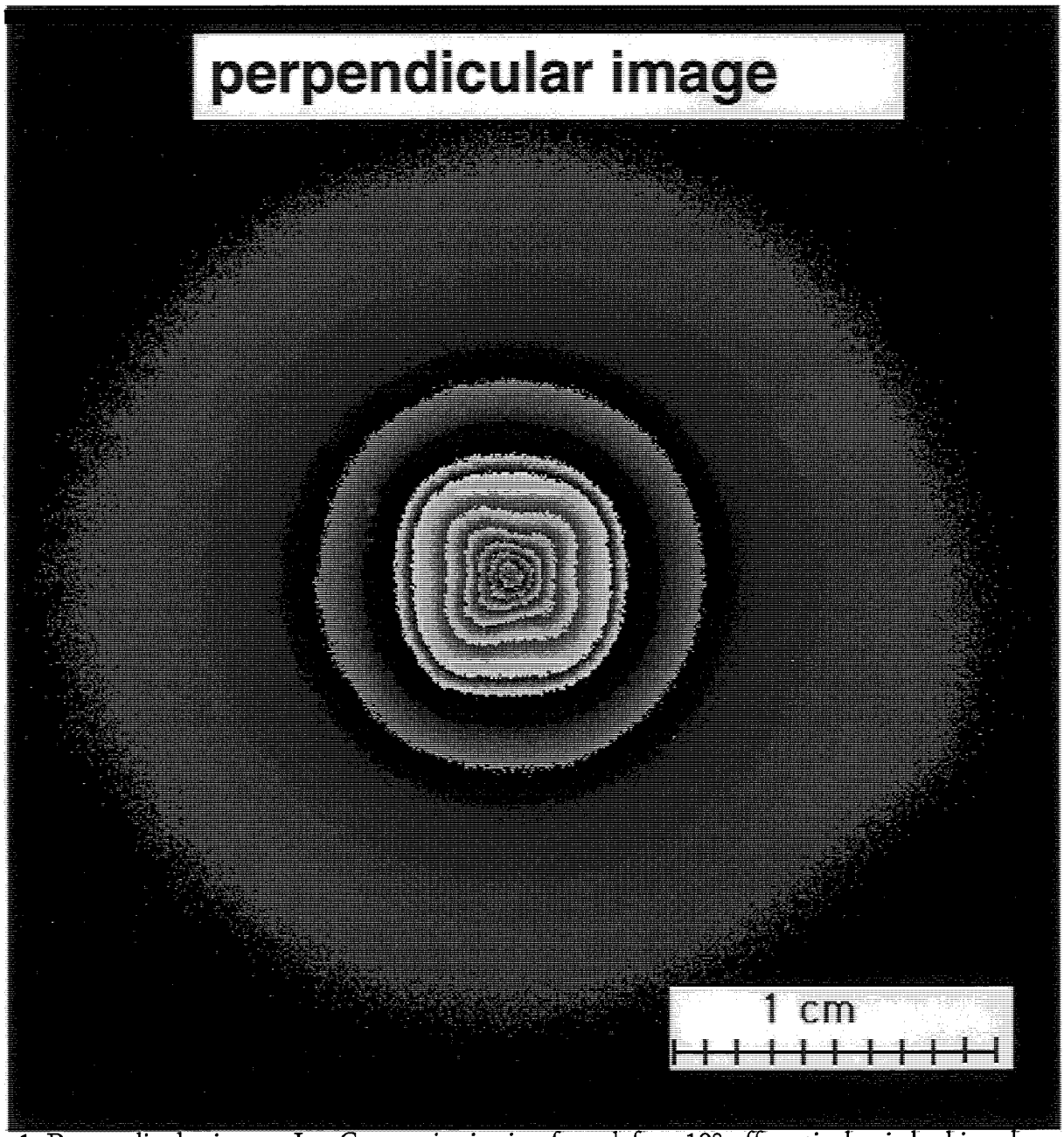

Fig. 1 Perpendicular image, $I_{=}$. Camera is viewing from left at 10° off vertical axis looking down at phantom. Source polarization is parallel with reference plane (connecting camera at left and laser beam straight up out of plane of page). Polarizing filter in front of camera is perpendicular to reference plane.

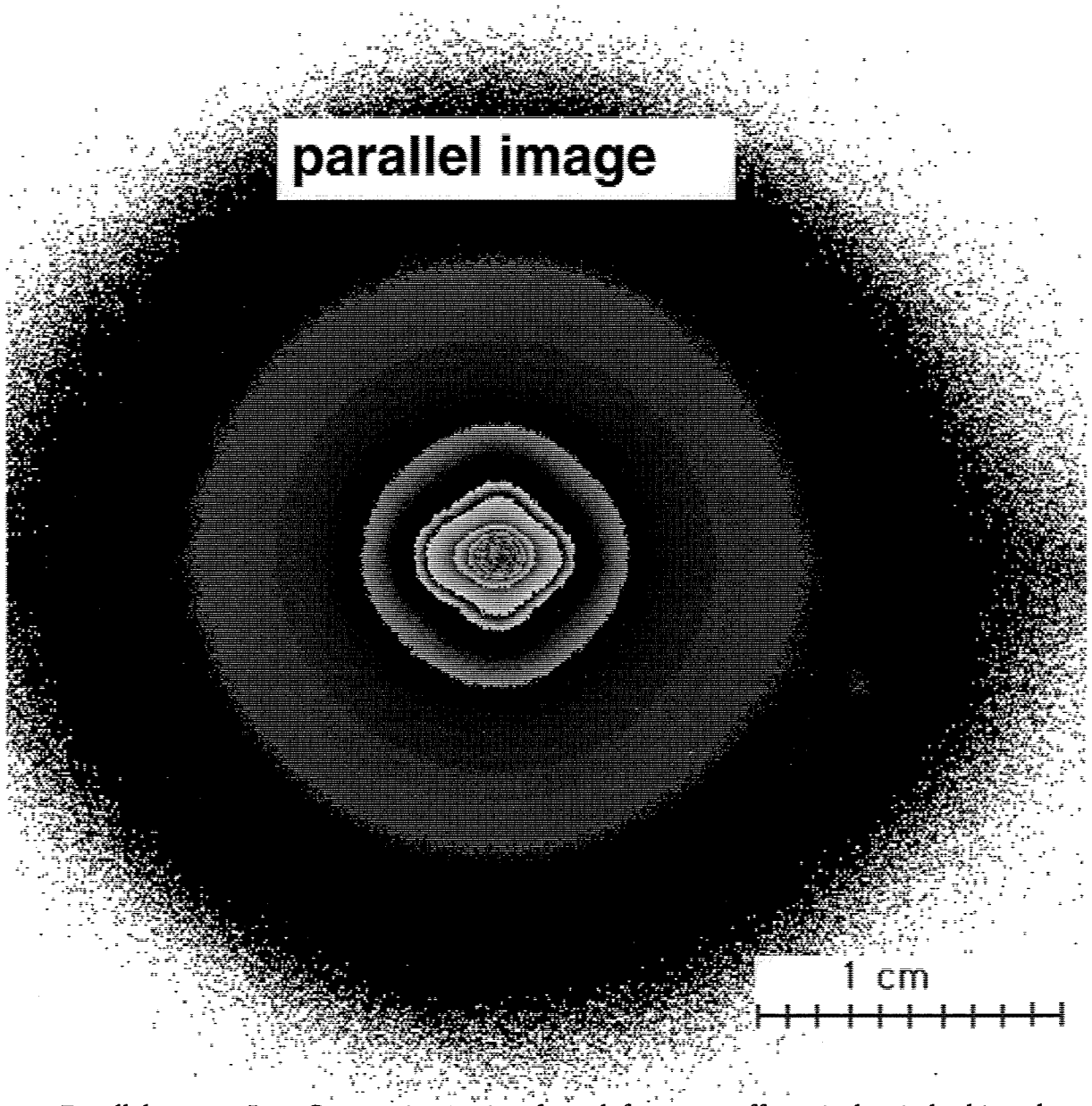

Fig. 2 Parallel image, $I_{\perp}$. Camera is viewing from left at 10° off vertical axis looking down at phantom. Source polarization is parallel with reference plane (connecting camera at left and laser beam straight up out of plane of page). Polarizing filter in front of camera also parallel to reference plane.

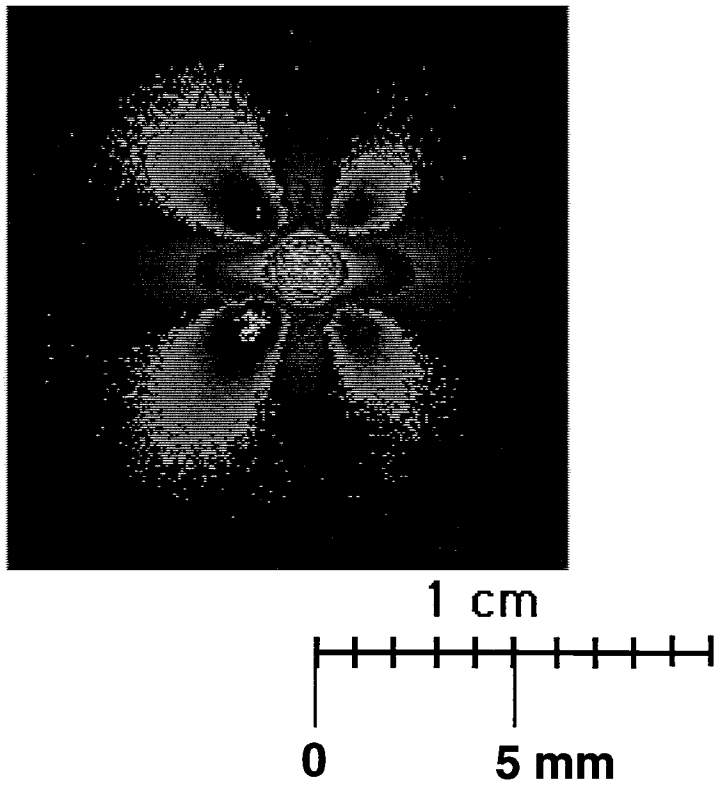

Fig. 3 Difference image, $I_{=} - I_{\perp}$.

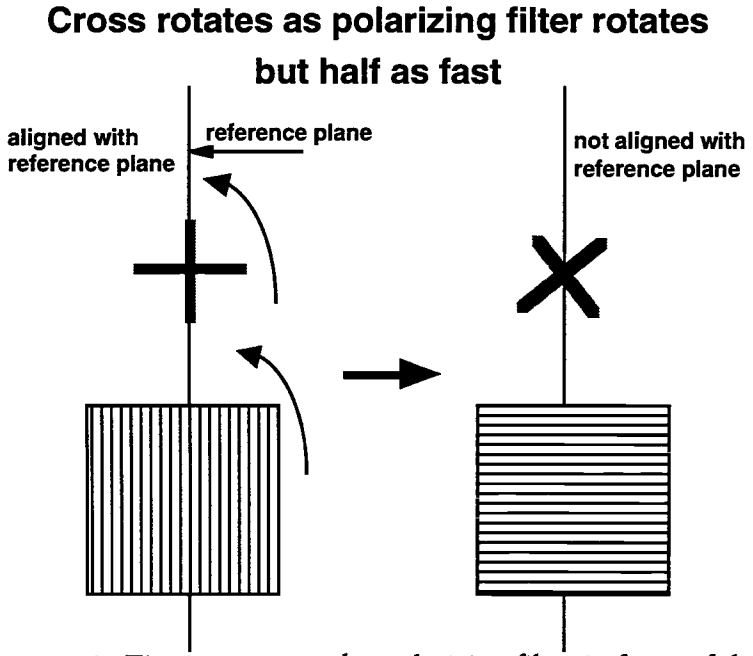

Fig. 4: Cross shape seen in Fig. 3 rotates as the polarizing filter in front of the camera is rotated. But the rotation is only half as fact as the filter rotation.

Optical fiber measurements with a polarized source and omni-polarized collection

Fig. 5 shows the results of the optical fiber measurements of linearly polarized light escaping at the air/medium surface of the phantom.

Near the source, the polarization strongly affects light transport to the collector. Far from the source, the polarization does not influence light transport.

We noted that the video measurements, where polarization was varied at the detector and the source was parallel to the reference plane, caused parallel images to be greater in signal amplitude near the source than the perpendicular signal. In contrast, the optical fiber measurements, where polarization was selected at the source and the collection fiber collected both polarization equally, the perpendicular-source signal was stronger than the parallel-source signal.

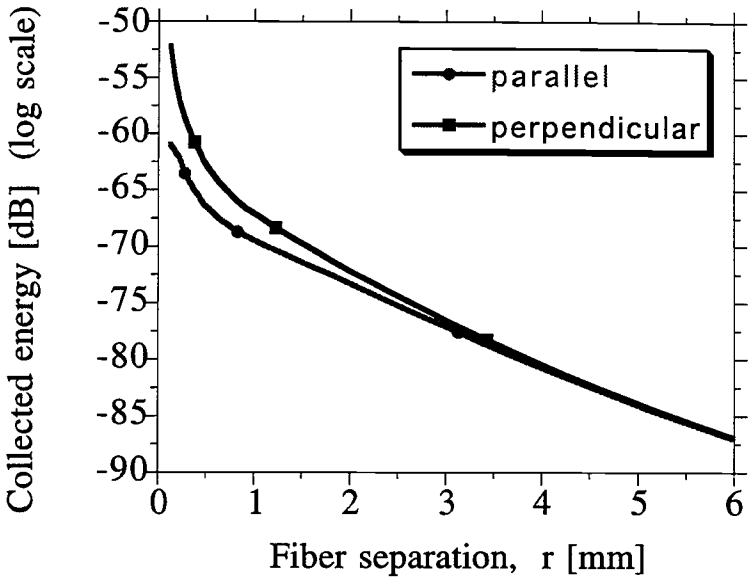

Fig. 5: NEAR THE SOURCE: *Source is polarized diode laser and source fiber is single mode; collector is multimode fiber.* The transport of polarized light extends to about 4.3 mm. (y-axis is logarithmic scale.) Light parallel to the reference plane is less efficiently transported than light perpendicular to the reference plane. As r increases, the both parallel and perpendicular polarization propagates equally well.

5. DISCUSSION

The video results showed that the strongest polarization occured within about 0.35 cm of the 633-nm source (0.35(0.20 + 6.07) = 2.2 mfp', where mfp' = $1/(\mu_a + \mu_s')$). The fiber results showed that the polarization escaped within about 0.43 cm of the 792-nm source (0.43(0.020 + 5.14) = 2.2 mfp'). The conclusion is that polarization extends about 2.2 transport mean free paths (mfp').

Table 2: Extent of polarization in phantom			
	transport mean free path (mfp')	polarized extent (cm)	expressed in mfp'
633 nm	0.159 cm	0.35 cm	2.2
792 nm	0.194 cm	0.43 cm	2.2

For the skin in the red to near-infrared wavelength range, the scattering is $\mu_s' \approx 15$ cm^{-1} and the absorption is $\mu_a \approx 0.25$ cm^{-1}, which yields a mfp' of 0.066 cm. Therefore 2.2 mfp' is about 1.5 mm. Light can propagate in water 1.5 mm in about 6.4 ps. This suggests that polarization imaging would provide the equivalent of a 6.4-ps time-gate for acceptance of light that contributes to the image.

The depth of interrogation within this 5.3-ps time-gated image can be estimated using classical paths (Feynman paths) to predict photon trajectories. The furthest that photons could travel would be 1.2 mm and exit at distances closer to the source at the same 5.3 ps time point would allow photons to travel deeper into the tissue. Hence, the Fig. 6 provides an upper estimate of the depth of probing by polarization imaging using red to near-infrared wavelengths. Shorter wavelengths have shorter mfp' and therefore would interrogate more superficially.

While polarization images were generated in phantoms, generation of such images in skin is still in progress. The size distribution of scatterers in skin includes smaller scatterers and the skin is not simply a homogeneous medium of 0.900-μm-diameter spheres. In a study by Schmitt et al. 1991 using circularly polarized light, smaller particles (0.22 μm spheres) were reported to attenuate lateral spread of circularly polarized light more strongly than larger particles (1.03 μm spheres).[1] The differences between linearly and circularly polarized light need to be considered. Also, the use of shorter wavelength light for imaging may increase the particle size-to-wavelength ratio and increase the ability to generate polarization images in the reflectance mode. More work on optimizing polarization imaging of the skin using backscattered short-path photons is still needed.

Advantage of polarization imaging

The advantage of polarization images are that they measure the superficial layer of a tissue and reject the large amount of diffusely scattered light. By delivering light at different angle than the angle of the camera, specular reflectance from the skin surface can be rejected. Alternatively, one can scan a polarized beam while acquiring the field of polarized reflectance escaping laterally from the point of photon injection. Either way, the images would not be blinded by either specular reflectance or diffuse reflectance. The mechanism of contrast would be the optical absorption and scattering and birefringence of the superficial skin. Any heterogeneity in the tissue would upset the pattern expected for a homogeneous tissue, and such discrepancies could be highlighted by false-color images superimposed on a diffuse light image of the tissue.

The ability to translate the results from the phantom experients (polystyrene spheres as scatterers) to skin (keratin and collagen fibers as scatters, plus contributions from sub-micron structures in cells) must be tested experimentally. We are just beginning to apply the technique to in vivo skin imaging.

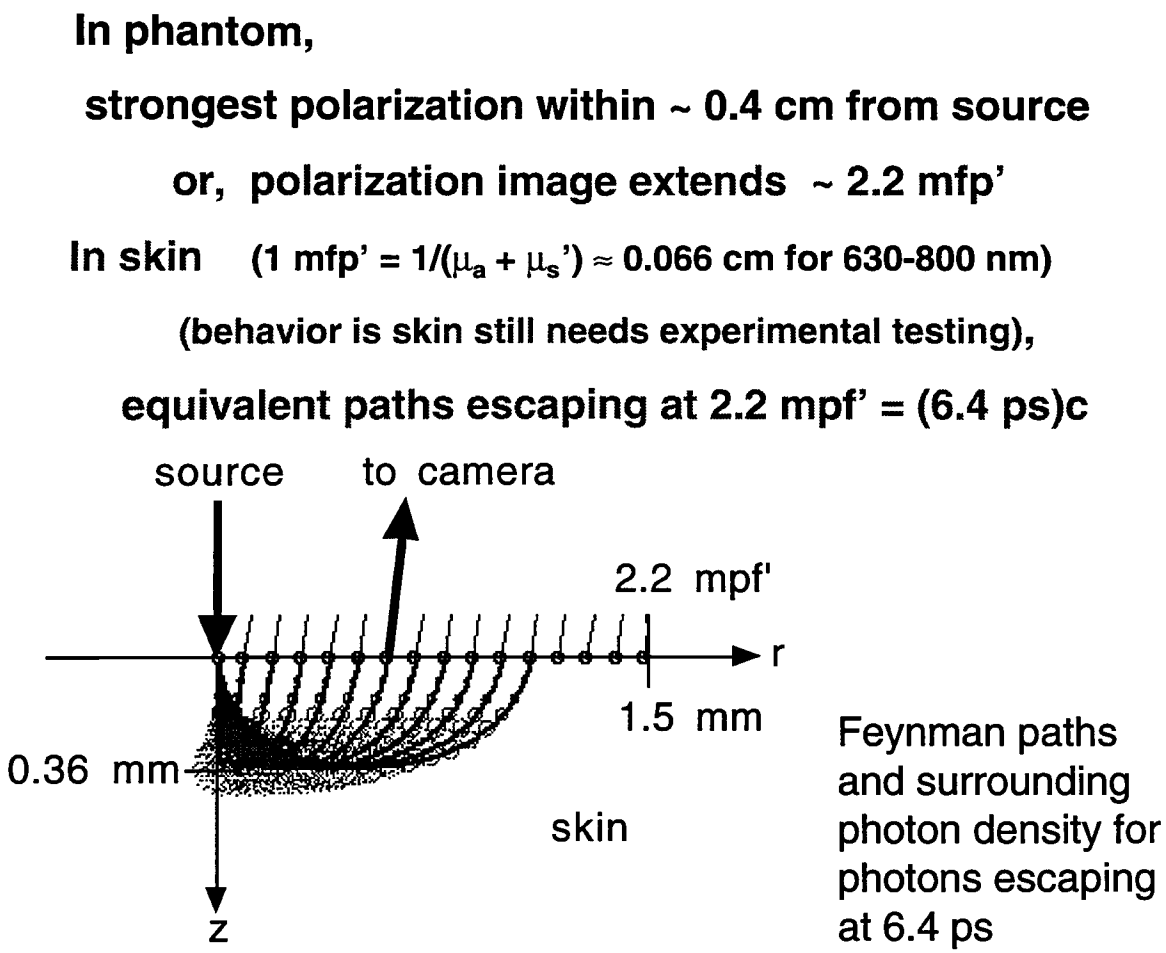

Fig. 6: Depth of interrogation by polarization imaging using red to near-infrared light. Predictions of most probable photon paths are predicted by classical paths (Feynman paths). Photons that moved directly across the surface within the tissue would arrive at 1.5 mm at 6.4 ps before escaping (relatively unlikely paths). The most probable paths that exit at 6.4 ps are closer to the source, as shown. The classical paths are solid lines. The dotted circles around these classical paths indicate the growth and collapse of a Gaussian spread around the classical path, indicating the region of most likely photon residence. The maximum depth of the classical paths is 360 μm.

Conclusions:

- **Polarization images based on lateral spread of polarized light:**
  - **utilize short-path photons**
  - **reject the dominant diffuse light**
  - **avoid specular reflectance**
- **Red and near-infrared could image within 300 μm and shorter wavelengths (eg., blue light) would be even more superficial**

6. ACKNOWLEDGEMENTS

This work was supported by the NIH (R29-HL45045) and the Dept. of Energy (DE-FG03-95ER61971).

7. REFERENCES

1 J.M. Schmitt, A.H. Gandjbakhche, R.F. Bonner: Use of polarized light to discriminate short-path photons in a multiply scattering medium. *Applied Optics,* 31:6535-6546, 1992.